PHYSICAL REVIEW C VOLUME 44, NUMBER 3 SEPTEMBER 1991

Heavy fragment emission in alpha-induced reactions on aluminum at 60 MeV

C. Bhattacharya, S. K. Basu, S. Bhattacharya, A. Chakrabarti, S. Chattopadhyaya, M. R. DuttaMajumdar, K. Krishan, G. S. N. Murthy, B. Sinha, M. D. Trivedi, and Y. P. Viyogi
Variable Energy Cyclotron Centre, 1/AF Bidhan Nagar, Calcutta 700064, India

S. K. Datta*
Saha Institute Of Nuclear Physics, 1/AF Bidhan Nagar, Calcutta 700064, India

R. K. Bhowmik
Nuclear Science Centre, New Delhi 110067, India
(Received 7 September 1990)

The production of intermediate-mass fragments ranging from $Z=3$ to 8 emitted in the reaction of 60 MeV alpha on an aluminum target has been experimentally studied. The energy spectra of the emitted fragments in the angular range of 20°–130° have been measured and the total production cross sections of each fragment have been estimated from the data. The double-differential cross-section data have been compared with the predictions made using (a) a phenomenological moving source model and (b) a binary fragmentation model. The absolute total emission cross sections for various fragments have been calculated assuming the statistical decay of a fully equilibrated compound nucleus and have been compared with the corresponding experimental estimates. It is found that the exit-channel deformation plays a significant role in the estimation of the Coulomb barrier of the separating nuclei. A theoretical procedure for the estimation of the exit-channel Coulomb barrier for the deformed system has been incorporated in the present calculation.

I. INTRODUCTION

In recent years, the intermediate-mass fragments (IMF) emitted in low- and intermediate-energy nucleus-nucleus collisions have been a subject of intense theoretical and experimental studies. A large amount of data from recent measurements of IMF emission are already available in the literature [1–8], and several theoretical models [8–12] have been proposed to understand the origin of these IMF's emitted in different reactions. Phenomenological analyses [8] of the data indicate that there may be a number of different reaction mechanisms which play significant roles in explaining the IMF emission depending on the incident energy of the projectile as well as the target-projectile combination. In the case of reactions induced by high-energy protons, the production cross section of a particular element of atomic number Z has been found to obey a simple power law of the form $\sigma(Z) \propto Z^{-N}$ [13], which has been interpreted as a signature for the occurrence of statistical clustering near a critical point [14–16]. At low bombarding energies these fragments ($3 \leq Z \leq 15$) are assumed to originate from the statistical decay of a fully equilibrated compound nucleus (CN) [4]. For lighter composite systems ($A \leq 50$), an asymmetric binary fragmentation model where the fully equilibrated composite system fragments into two unequal parts [9,10] due to the dynamical deformation of the composite system has also been found to be quite successful in explaining the general trend of the data. However, at higher energies (≥ 15 MeV/nucleon), it has been found that emission from the fully equilibrated compound nuclear source may not be sufficient to explain the whole range of the data and it may be necessary to incorporate the effects of IMF emission from other intermediate velocity sources, moving with velocities intermediate between the incident projectile velocity and the compound nuclear velocity [17–22]. Moreover, there are IMF emissions from the targetlike and the projectilelike sources and these introduce further difficulties in unfolding the contributions from each individual source to compare with the respective theoretical predictions. In this respect, light-ion-induced reactions have an advantage; IMF's emitted in these reactions are little contaminated by the emission from projectilelike and targetlike sources and therefore can be directly compared with the theoretical predictions to extract valuable information regarding the reaction mechanisms dominant in that energy regime. In recent years, a large number of measurements of IMF emissions have been done [20–23] in the energy range of 20–30 MeV/nucleon; however, few measurements have been reported at lower energies.

We report here the measurements of energy spectra and angular distribution for various IMF's ($3 \leq Z \leq 8$) emitted in 60 MeV α-induced reaction on a ^{27}Al target. The experiment was performed at the Variable Energy Cyclotron Centre, Calcutta. The experimental details and the general nature of the energy spectra, angular distributions, total cross section, etc., will be described in Sec. II. In Sec. III the analysis of the data in terms of moving source and binary fragmentation models will be presented. A theoretical evaluation of the deformation in exit channel and its effect on the barrier will also be described in detail in Sec. III. A summary of the results and the present outlook on possible mechanisms is given in Sec. IV.

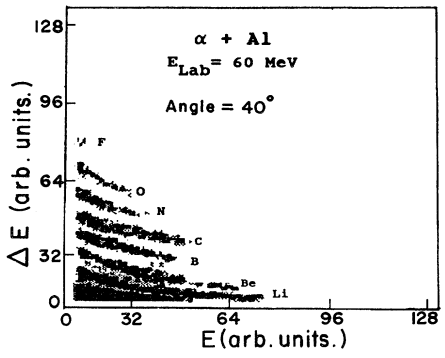

FIG. 1. Two-dimensional ΔE vs E spectra for the heavy fragments detected in 60 MeV $\alpha+^{27}$Al reaction at the detection angle of 40°.

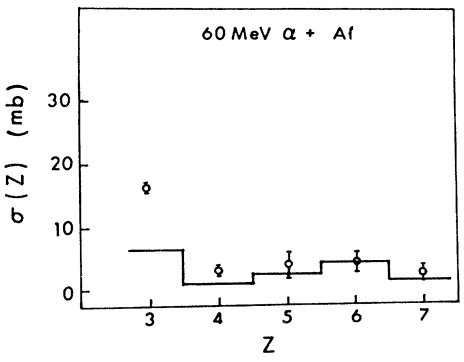

FIG. 2. Total cross sections $\sigma(Z)$ as a function of atomic number Z of the detected fragments. The solid histogram represents the theoretical predictions obtained using the binary fragmentation model.

II. EXPERIMENTAL PROCEDURE AND RESULTS

The experiment was performed at the Variable Energy Cyclotron Centre, Calcutta, using 60 MeV α particle on a ^{27}Al target. The target was made of an aluminum foil of thickness 810 μg/cm^2 having a uniformity of better than 5%. The different mass fragments were identified using a gas ΔE-silicon-E (thickness = 300 μm) telescope. To reject the energetic lighter ($Z \leq 2$) particles, a silicon veto detector was used at the back of the E detector. The gas

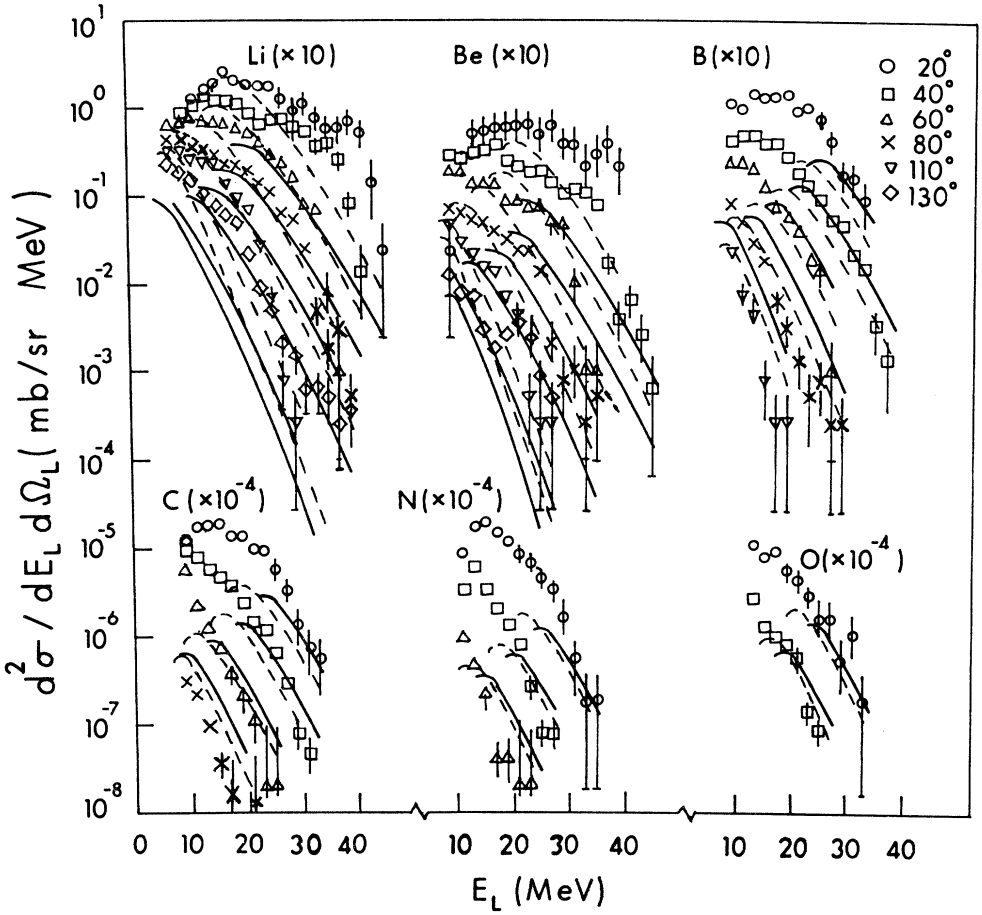

FIG. 3. Double-differential cross sections for fragments lithium to oxygen emitted in the reaction 60 MeV $\alpha+^{27}$Al as a function of the laboratory energy (E_L) of the fragments. Solid lines represent the results of the binary fragmentation model where the Coulomb barrier E_B has been calculated using spherical exit-channel configuration (see text). The dashed line represents the same calculation, where E_B was obtained from individual best fits of the experimental data.

telescope was of axial configuration having an active length of 4 cm and filled with a continuous flow of P10 gas (90% Ar + 10% CH_4) at 130 torr nominal pressure [24]. Gas pressure was maintained constant to within ±2 torr. A thin polypropylene film of thickness 1.5–2.0 μm was used for the window of the gas detector. The gas telescope subtended a solid angle of 1.2 msr and had angular opening of 1°. For the present measurement, two such (ΔE-E) telescopes were used, which were placed on two different arms of the 900-mm scattering chamber, so that each of them could be rotated independently for the angular distribution measurements. Analog signals from the detectors were properly processed using standard electronics before being fed to the computer for on-line data acquisition. Data were recorded in the event-by-event mode on magnetic tape using a CAMAC-based data-acquisition system [25] on Norsk Data ND-560 computer, which was later analyzed off-line.

The charge resolution obtained using this telescope has been described in detail elsewhere [24]. The charge resolution obtained in this experiment is illustrated by the ΔE vs E plot displayed in Fig. 1. Well-separated ridges are clearly seen corresponding to elements having atomic numbers up to $Z=9$. The telescopes have been calibrated using recoil ions of Li and C produced by bombarding 60 MeV α particle on a mixed target (125 μg/cm^2 LiF on 25 μg/cm^2 carbon backing). Absolute energy calibrations of the E and ΔE detectors were done separately using standard kinematics and energy-loss calculations. Typical energy resolutions obtained in the recoil calibration were 3.9% and 9.7% for E and ΔE detectors, respectively. The measured energies have been corrected for the energy losses at the target and at the entrance window by incorporating a single average thickness correction for each fragment energy in the following manner. For each fragment, total energy loss in one-half thickness of the target (assuming that the fragments are produced at the center of the target on the average) and full thickness of the entrance window, calculated over the range of incident energies of our interest, was parametrized as a function of the detectable energy (incident energy minus total energy loss). Experimentally measured energies were then suitably corrected for the energy losses using the proper functional forms corresponding to each fragment. Experimental cutoffs thus obtained are typically 6 MeV for lithium and 13 MeV for oxygen. Carbon build-up on the target was monitored at regular intervals and was found to be negligible.

Total elemental cross sections as a function of Z obtained from the reaction 60 MeV $\alpha+^{27}$Al are shown in

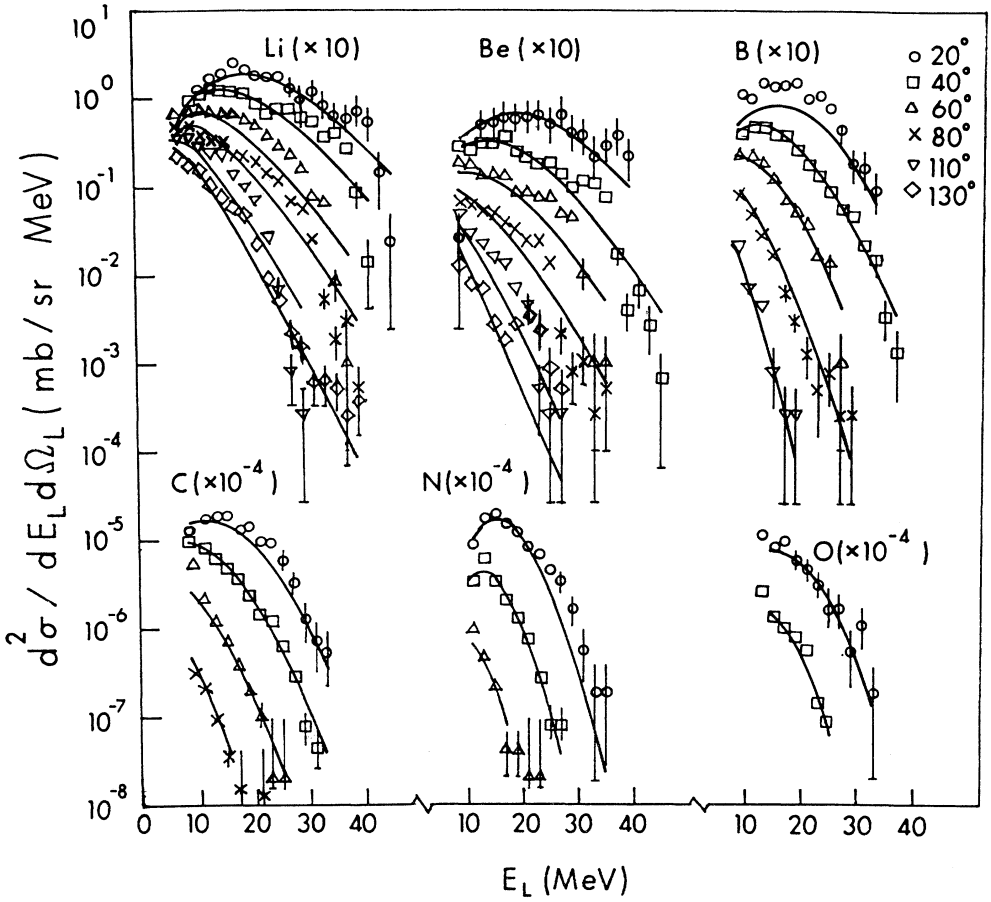

FIG. 4. Double-differential cross sections for fragments lithium to oxygen emitted in the reaction 60 MeV $\alpha+^{27}$Al as a function of the laboratory energy (E_L) of the fragments. The solid line represents the fit obtained using the moving source model.

Fig. 2. Except for Li, all other cross sections vary with much smaller gradient compared to those obtained earlier at higher incident energies [1]. The energy spectra for various IMF's ($3 \leq Z \leq 8$) are shown in Figs. 3 and 4 for different angles. The error bars shown represent only statistical errors. The other errors which contribute to the cross section are mainly due to the determination of solid angle by geometrical method and the calibration of the current digitizer, which are around 10%.

III. ANALYSIS AND DISCUSSION

A. Total elemental cross sections

Theoretically, the total IMF cross section can be estimated from simple phase-space consideration. Assuming that the projectile and the target fuse completely to form an excited compound nucleus before it decays into various channels which are energetically possible, and that the decay is purely statistical in nature, the total emission cross section for a particular channel specified by its atomic number Z can be written as

$$\sigma(Z)=\pi\lambda\!\!\!^{-2}\sum_{l=0}^{l_{\rm crit}}(2l+1)\Gamma_Z/\Gamma_{\rm tot}\ , \tag{1}$$

where $l_{\rm crit}$ is the critical angular momentum for fusion and $\lambda\!\!\!^{-}$ is the de Broglie wavelength. The ratio $\Gamma_Z/\Gamma_{\rm tot}$ represents the probability of decay of the compound nucleus in any particular channel with atomic number Z and Γ_Z is given by [4]

$$\Gamma_Z(l)\propto T_Z[E/(E-B_Z)]^2\exp\{2[a(E-B_z)]^{1/2}-2(aE)^{1/2}\}\ . \tag{2}$$

E is the compound nucleus excitation energy and B_Z is the barrier height at the conditional saddle point. The level density parameter a is taken to be $\simeq A_{\rm CN}/8$ and the temperature T_Z is calculated from the relation $E-B_Z=aT_Z^2$. The conditional saddle point has been evaluated by minimizing the potential energy of the deformed compound system [26], assuming the rotating liquid-drop model for the nuclear potential and the proximity nucleus-nucleus interaction of Swiatecki [27]. The prediction of the present calculations has been displayed in Fig. 2 along with the respective experimental estimates for comparison. The experimental cross sections represented by circles have been obtained by integrating the double-differential cross-section data over the whole energy and angular range in the following way. Energy integration for each angle has been done by generating an interpolation function passing through all experimentally measured data points, which have then been extrapolated to the energies below the experimental threshold with the additional constraint that the function should be zero at zero energy. This function has then been numerically integrated to obtain energy-integrated angular distributions for the fragments. These angular distributions have been finally fitted by smooth polynomial functions and numerically integrated to give total elemental cross sections for the fragments. The combined uncertainties due to experimental threshold and the limited angular range of the data have been estimated to be 10% for Li, 17% for Be, 45 % for B, 41% for C, and 50% for N.

It is seen that the total absolute cross sections predicted by the present model based purely on statistical consideration (shown by solid histogram in Fig. 2) are in good agreement with the corresponding experimental values except for lighter fragments where the theoretical predictions are seen to underestimate the experimental values. This may be indicative of the fact that the heavier fragments are emitted from a nearly equilibrated compound nucleus, whereas processes other than purely statistical ones may play a significant role in the emission of lighter fragments.

B. Fragment energy distribution

1. Binary fragmentation model

Asymmetric binary splitting of the compound nucleus [9] is presently being considered as one of the dominant reaction mechanisms for the IMF emission in the low- and intermediate-energy domains. According to this model, the energy distribution $P(X)$ of the fragments in the center-of-mass system (c.m.) is given by

$$P(X)dX\cong X\exp(-X/T)\ , \tag{3}$$

where $X=E_{\rm c.m.}^{\rm kin}-E_B$ is the total kinetic energy in the c.m. above the barrier and T is the temperature as defined earlier. The exit-channel Coulomb barrier E_B is given by

$$E_B=1.44Z_1Z_2/[r_0(A_1^{1/3}+A_2^{1/3})+d]\ , \tag{4}$$

where $r_0=1.18$ fm and d ($\simeq 2$ fm) is the surface-to-surface separation between the two fragments having mass numbers A_1, A_2 ($=A_{\rm CN}-A_1$) and atomic numbers Z_1, Z_2 ($=Z_{\rm CN}-Z_1$), respectively, at the conditional saddle point.

Incorporating the effect of entrance-channel angular momentum, the double-differential cross section for various fragments can be written as

$$d^2\sigma/dE_L d\Omega_L=\pi\lambda\!\!\!^{-2}\sum_{l=0}^{l_{\rm crit}}(2l+1)(\Gamma_Z/\Gamma_{\rm tot})d^2P/dE_L d\Omega_L\ , \tag{5}$$

where the probability distribution $d^2P/dE_L d\Omega_L$ in the laboratory has been obtained from the c.m. probability distribution [Eq. (3)] using a standard transformation technique [1].

The expression (5) for the differential cross section has been obtained under the assumption that the fragment angular distribution in the c.m. is isotropic. However, it is well known that the fission fragment angular distributions show a $1/\sin\theta_{\rm c.m.}$ type of dependence. Since the binary fragmentation process described here is very much similar to the fission process, it may be quite reasonable to assume that the binary fragment angular distribution should also have a similar kind of angular dependence. In the present calculation, it has been taken care of in an approximate manner by including an additional $(1/\sin\theta_L)$ dependence in Eq. (5). Energy spectra of

TABLE I. Comparison of the exit-channel Coulomb barriers for spherical and deformed exit-channel shapes with those obtained from the analysis of the experimental data.

Z	Eccentricity	Coulomb barrier E_B Spherical	Deformed	From expt.
3	0.845	6.76	4.86	4.73±0.35
4	0.842	8.16	5.92	6.28±1.1
5	0.840	9.19	6.68	6.52±0.85
6	0.839	9.90	7.22	6.86[a]
7	0.838	10.23	7.48	7.77[a]

[a]Uncertainties not estimated.

different fragments have been calculated using Eq. (5) and are shown in Fig. 3 by solid lines along with the experimental data. From this figure, it is evident that the data for the heavier fragments (B,C,N,O) are in fair agreement with this model prediction at energies greater than the barrier energy E_B (Table I, third column). The model predictions are in fair agreement with the slopes of energy spectra, at higher angles ($>40°$) for lighter fragments (Li,Be). This suggests that the emission of heavier fragments as well as the emission of lighter fragments at higher angles may be taking place from binary fissionlike decay of nearly equilibrated compound nucleus.

Thus, it is clear from the above discussion that the present distribution [Eq. (3)] is not quite adequate for a proper quantitative explanation of the data over the whole angular range, even though the total reaction cross sections for most of the fragments can be very well predicted from simple phase-space considerations. Part of this inadequacy is definitely due to the noninclusion of the exit-channel deformation in the calculation, as will be discussed in the next subsection. On the other hand, a basic inadequacy of the distribution itself may not also be ruled out, which calls for a systematic investigation using more experimental data with several targets and for a range of energies.

2. *Moving source model*

The experimental energy spectra shown in Fig. 4 (same as those in Fig. 3) exhibit smooth exponential slopes which vary slowly from fragment to fragment. A simple, intuitive understanding of the data can be had in the phenomenological moving source model [19], where it was assumed that the fragments are emitted isotropically in the rest frame of a source moving with velocity V_0. In the laboratory rest frame, the double-differential fragment emission cross section can be written as [19]

$$d^2\sigma/dE_L d\Omega_L = C[(E_L - E_B)E_{SX}]^{1/2}\exp(-E_{SX}/T) , \tag{6a}$$

with

$$E_{SX} = (E_L - E_B) + E_0 - 2[E_0(E_L - E_B)]^{1/2}\cos\theta_L \tag{6b}$$

and

$$E_0 = \tfrac{1}{2} m_F V_0^2 , \tag{6c}$$

where C is normalization constant, E_L and m_F are the laboratory energy and mass of the emitted fragment, θ_L is the detection angle in the laboratory, T is the slope (temperature) parameter, and E_B corrects for the Coulomb repulsion from the target residue.

To have a phenomenological understanding about the nature of sources from which the fragments are assumed to be emitted, the present data have been fitted with the empirical relation given by Eq. (6a). A visual inspection of the data (Fig. 4) reveals that for all fragments, the energy distributions obtained for various angles are qualitatively similar except for the forward angle (20° and 40°) distributions of Li and Be, which exhibit a somewhat different trend. Therefore, for each fragment, all the data have been fitted simultaneously to extract a unique set of source velocity and temperature parameters corresponding to that fragment, whereas for Li and Be, the forward angles (20° and 40°) and the rest of the data have been fitted separately to understand the nature of the sources in respective angular regions.

The predicted cross sections corresponding to the best-fit parameters have been displayed (solid line) along with the respective experimental data in Fig. 4 for comparison. It is clear from Fig. 4 that the simple parametrization as described above is able to explain the data reasonably well. The variation of source velocity and temperature parameter as a function of atomic number of the emitted fragments are given in Table II. It is found that except or Li and Be at forward angles ($\leq 40°$), source velocities extracted for different fragments are nearly the same and are quite close to the corresponding compound nuclear value. This suggests that all these fragments may

TABLE II. Velocity and temperature parameters obtained from the phenomenological moving source model analysis of the IMF emission cross sections for the reaction $\alpha + {}^{27}$Al at 60 MeV.

Z	Angular range	V_0/V_{CN}	T
3	$\leq 40°$	1.83±0.31	3.42±0.36
	$>40°$	1.25±0.08	3.80±0.15
4	$\leq 40°$	1.83±0.33	2.59±0.31
	$>40°$	1.42±0.11	3.42±0.25
5	All	1.37±0.03	2.05±0.07
6	All	1.33±0.03	1.79±0.10
7	All	1.25±0.03	0.98±0.05
8	All	1.29±0.06	1.08±0.16

be emitted from a compound-nucleus-like source. On the other hand, the forward angle ($\leq 40°$) emissions for Li and Be may have significant contributions from the sources other than compound-nucleus sources having velocities differing considerably from that of the compound nucleus (Table II). This is in agreement with the analysis made in the preceding subsection using the binary fragmentation model. The moving source parameters extracted from fitting the data may have some variations depending on how the energy spectra have been corrected for the energy loss in the target and the entrance window of the detector. To see how the source parameters depend on the magnitude of the energy-loss correction, we have repeated the calculation for another extreme case where the energy-loss correction due to the full thickness of the target (instead of one-half thickness of the target as had been done throughout the present paper) was incorporated in the extraction of fragment energy spectra. However, in this case, it has been found that the source parameters do not depend strongly on the magnitude of the energy-loss correction (variations $V_0/V_{\rm CN} \sim 3-4\%$, $T \sim 8-9\%$).

C. The effect of deformation in the exit channel

A closer comparison of the theoretical prediction of Eq. (5) and the experimental data reveals that the maxima of the energy spectra do not match properly. The shapes are better reproduced by allowing the Coulomb barrier E_B to vary. The results of a least-squares fit of the data with Eq. (5) by varying E_B are shown by dashed lines in Fig. 3. The E_B values obtained from a least-squares fit are always found be be smaller than those obtained from Eq. (4) where the separating fragments have been assumed to be spherical in shape (see Table I). To reproduce the experimental E_B values using Eq. (4) requires a value of $r_0 \simeq 1.56$ fm. Such a large value for r_0 is indicative of large deformation in the exit channel. Such deformations are quite common in the fission of actinides [28]. Moreover, a recent analysis of the IMF cross-section data using the sum-rule model [8,11] reports values for r_0 in the range 1.5–1.7 fm. It is thus clear that the exit-channel barrier may give valuable information regarding the actual deformation of the system at the time of separation.

The effect of exit-channel deformation on the Coulomb barrier between the two fragments at the time of separation can be estimated in the following manner. We assume that after reaching the conditional saddle point, the two nuclei (subsequently emitted as fragments) begin to deform until the center-to-center distance between the two is equal to r_d, called deformation radius [29], and is defined as

$$r_d = r_i + (r_i - r_c) , \tag{7}$$

where r_i is the interaction radius [30] of two separating nuclei and r_c is the minimum distance between the two nuclei at the conditional saddle point, defined as

$$r_c = c_1 + c_2 + d . \tag{8}$$

Here c_1 and c_2 are the half-density radii [30] of the two separating fragments and d is the surface-to-surface separation distance at the conditional saddle point. This surface-to-surface separation is kept constant ($\simeq 2$ fm) throughout the time the nuclei are allowed to deform. The deformed nuclei are assumed to be prolate ellipsoids with their symmetry axes along the line joining the centers. Then, the distance between the centers at the limiting deformation is given by

$$r_d = a_1 + a_2 + d , \tag{9}$$

where a_1 and a_2 are the semimajor axes of the two separating fragments at the limiting deformation.

Assuming that the deformation is volume conserving and that the eccentricity ε of the two nuclei is the same, it is then possible to calculate the exit-channel deformations and barrier for each binary combination which can be compared with the corresponding best-fit barriers obtained from experimental data. The exit-channel Coulomb barrier for the deformed system can then be written as

$$E_B = Z_1 Z_2 e^2/(a_1 + a_2 + d) + \Delta W , \tag{10}$$

where ΔW is the higher order correction [29] to the barrier E_B.

The values of E_B calculated for spherical and deformed shapes as well as the best-fit values of E_B obtained from the experimental data for various fragments are given in Table I for comparison. The values of ε calculated in the above formalism for different binary fragment combinations have also been included in Table I. From this table it is clear that the values of E_B obtained for the deformed systems are significantly smaller than those obtained for the corresponding systems when the separating fragments are assumed to be spherical in shape. Moreover, from Table I, it is clear that the barriers calculated using the present prescription are quite close to the individual best-fit barriers obtained from the analysis of the experimental data.

IV. SUMMARY AND CONCLUDING REMARKS

The inclusive double-differential cross sections for fragments ranging from lithium to oxygen emitted in the reaction $\alpha + {}^{27}$Al at 60 MeV have been measured. Total emission cross sections for various fragments emitted in the above reaction have been computed from the double-differential cross-section data. Total emission cross sections for various fragments are very well explained by the statistical emission from a fully equilibrated compound nucleus. For lighter fragments, however, the model underestimates the data which may be indicative of the significant contribution of reaction mechanisms other than the fully equilibrated one in the case of lighter fragments emission. Binary splitting of the compound nucleus is found to explain the slopes of the double-differential cross-section data fairly well except for the lighter fragments (Li,Be) at forward angles; however, the absolute double-differential cross section predicted by this model is not in good agreement with the data over

the whole angular range. Considering the fact that the total emission cross sections are very well explained by simple statistical decay of the CN, this may be indicative of the inadequacy of the distribution function [Eq. (3)], and calls for further investigation. The discrepancy for the lighter fragments at forward angles in particular may, however, be due to contributions from nonequilibrium reaction mechanisms. Here neither the slopes of the energy spectra nor the total reaction cross sections are explained satisfactorily. This is further supported by the phenomenological moving source analysis which indicates that different fragments are emitted from different sources. Lighter fragments (Li,Be) at forward angles are found to be emitted from relatively hotter and faster sources whereas the heavier fragments (B,C,N,O) as well as lighter fragments (Li,Be) at intermediate and backward angles are emitted from colder sources whose velocities are quite close to the compound nuclear velocity. It suggests that a significant fraction of lighter fragments are emitted at the nonequilibrium stage of the reaction whereas the emission of heavier fragments may be taking place from a near-equilibrated compound nucleus.

Analysis of the data using the binary fragmentation model shows that there is a significant effect of exit-channel deformation. A large value of the radius parameter r_0 ($\simeq 1.56$ fm) obtained from fitting the individual best-fit barriers assuming spherical shapes for the separating fragments is indicative of such deformation. The effect of exit-channel deformation has been theoretically estimated in this calculation. It is found that the barriers obtained after including the deformation are in good agreement with the individual best-fit barriers obtained from the analysis of the experimental data. This suggests that the exit channel is not spherical but is considerably deformed. A quantitative measure of deformation is also obtained from the present analysis.

In conclusion, statistical decay of fully equilibrated compound nucleus can explain fairly well the total emission cross-section data for almost all the fragments, except for lighter ones like Li and Be. Energy distributions calculated using a binary fragmentation model are able to reproduce qualitatively the general features of the double-differential cross-section data, whereas the quantitative agreement is not very satisfactory. Phenomenological analysis of the data also indicates that reaction mechanisms for the emission of the lighter and heavier fragments may be different. In the case of the former, there may be contributions from hotter and faster sources in the cases of forward angle emission in particular, and the latter are mostly emitted from the nearly equilibrated compound nucleus. Moreover, the exit-channel deformation should also be properly taken into account for a proper explanation of the data. Further experiments as well as theoretical studies are necessary to have a better understanding of the reaction mechanisms which play important roles in this energy domain.

ACKNOWLEDGMENTS

The authors would like to thank S. K. Pardha Saradhi, R. P. Sharma, and S. N. Chintalpudi for their help in the preparation of the experiment. They would also like to thank the cyclotron operation staff and ND-560 computer personnel for their cooperation during the experimental run. Helpful discussions with J. N. De, D. K. Srivastava, and S. Pal are also acknowledged.

*Present address: Nuclear Science Centre, New Delhi 110067, India.

[1] T. Kozik, J. Buschmann, K. Grotowski, H. J. Gils, N. Heide, J. Kiener, H. Klewe-Nebenius, H. Rebel, S. Zagromski, A. J. Cole, and S. Micek, Z. Phys. A **326**, 421 (1987).

[2] K. Grotowski, J. Ilnicki, T. Kozik, J. Lukasik, S. Micek, Z. Sosin, A. Wieloch, N. Heide, H. Jelitto, I. Kiener, H. Rebel, S. Zagramski, and A. J. Cole, Phys. Lett. B **223**, 287 (1989).

[3] K. Kwiatkowski, J. Bashkin, H. Karwowski, M. Fatyga, and V. E. Viola, Phys. Lett. B **171**, 41 (1986).

[4] L. G. Sobotka, M. L. Padgett, G. J. Wozniak, G. Guarino, A. J. Pacheco, L. G. Moretto, Y. Chan, R. G. Stokstad, I. Tserruya, and S. Wald, Phys. Rev. Lett. **51**, 2187 (1983).

[5] L. G. Sobotka, M. A. McMahan, R. J. McDonald, C. Signarbieux, G. J. Wozniak, M. L. Padgett, J. H. Gu, Z. H. Liu, Z. Q. Yao, and L. G. Moretto, Phys. Rev. Lett. **53**, 2004 (1984).

[6] M. A. McMahan, L. G. Moretto, M. L. Padgett, G. J. Wozniak, L. G. Sobotka, and M. G. Mustafa, Phys. Rev. Lett. **54**, 1995 (1985).

[7] R. J. Charity, M. A. McMahan, G. J. Wozniak, R. J. McDonald, L. G. Moretto, D. G. Sarantites, L. G. Sobotka, G. Guarino, A. Pantaleo, L. Fiore, A. Gobbi, and K. D. Hildenbrand, Nucl. Phys. **A483**, 371 (1988).

[8] H. Rebel, I. M. Brancus, K. Grotowski, and T. Kozik, Proceedings of the Symposium on Nuclear Physics, Bombay, India [**31A**, 209 (1988)].

[9] L. G. Moretto, Nucl. Phys. **A247**, 211 (1975).

[10] L. G. Moretto and G. J. Wozniak, Nucl. Phys. **A488**, 337c (1988).

[11] I. M. Brancus, H. Rebel, J. Wentz, and V. Corcalciuc, Phys. Rev. C. **42**, 2157 (1990).

[12] M. Blann, T. T. Komoto, and I. Tserruya, Phys. Rev. C **40**, 2498 (1989).

[13] A. M. Poskanzer, G. W. Butler, and E. K. Hyde, Phys. Rev. C **3**, 882 (1971).

[14] P. J. Siemens, Nature **305**, 458 (1982).

[15] J. E. Finn, S. Agrawal, A. Bujak, J. Chuang, L. J. Gutay, A. S. Hirsch, R. W. Minich, N. T. Porile, R. P. Scharenberg, and B. C. Stringfellow, Phys. Rev. Lett. **49**, 1321 (1982).

[16] R. W. Minich, S. Agrawal, A. Bujak, J. Chuang, J. E. Finn, L. J. Gutay, A. S. Hirsch, N. T. Porile, R. P. Scharenberg, and B. C. Stringfellow, Phys. Lett. **118B**, 458 (1982).

[17] C. B. Chitwood, D. J. Fields, C. K. Gelbke, W. G. Lynch, A. D. Panagirton, M. B. Tasang, H. Utsunomiya, and W.

A. Friedman, Phys. Lett. **131B**, 289 (1983).
[18] C. K. Gelbke, Nucl. Phys. **A400**, 473c (1983).
[19] D. J. Fields, W. G. Lynch, C. B. Chitwood, C. K. Gelbke, M. B. Tsang, H. Utsunomiya, and J. Aichelin, Phys. Rev. C **30**, 1912 (1984).
[20] B. Borderie, J. Phys. (Paris) Colloq. **47**, C4-251 (1986).
[21] R. Dayras, J. Phys. (Paris) Colloq. **47**, C4-13 (1986).
[22] J. Hufner, J. Phys. (Paris) Colloq. **47**, C4-3 (1986).
[23] W. G. Lynch, Annu. Rev. Nucl. Part. Sci. **37**, 493 (1987).
[24] S. K. Bandyopadyay, S. K. Basu, S. Bhattacharya, R. K. Bhowmik, A. Chakrabarty, S. K. Datta, G. S. N. Murthy, and Y. P. Viyogi, Nucl. Instrum. Methods **A278**, 467 (1989).
[25] A. Bandyopadhyay, A. Roy. S. K. Dey, S. Bhattacharya, and R. K. Bhowmik, Nucl. Instrum. Methods **A257**, 309 (1987).
[26] C. Bhattacharya and S. Bhattacharya, Phys. Rev. C **43**, 1491 (1991).
[27] W. J. Swiatecki, LBL Report No. LBL-8950, 1979.
[28] R. Vandenbosch and J. R. Huizenga, *Nuclear Fission* (Academic, New York, 1973), p. 289.
[29] S. K. Samaddar, A. Sherman, D. Sperber, M. Zielinska-P'fabe, and J. N. De, Phys. Scr. **23**, 231 (1981).
[30] W. U. Schröder and J. R. Huizenga, Annu. Rev. Nucl. Sci. **27**, 465 (1977).